JOURNAL OF CHEMICAL PHYSICS VOLUME 109, NUMBER 13 1 OCTOBER 1998

Vibrational echo spectroscopy: Spectral selectivity from vibrational coherence

K. D. Rector, David Zimdars,[a] and M. D. Fayer[b]
Department of Chemistry, Stanford University, Stanford, California 94305

(Received 18 March 1998; accepted 25 June 1998)

Theory and experimental data are presented which illustrate a new method for performing two-dimensional vibrational spectroscopy using ultrafast pulsed infrared lasers, called vibrational echo spectroscopy (VES). The VES technique can generate a vibrational spectrum with background suppression using the nonlinear vibrational echo pulse sequence. The vibrational echo pulse sequence is used with the delay between the excitation pulses fixed while the excitation wavelength is varied. A detailed theory of VES is presented which calculates the full third order nonlinear polarization including rephasing and nonrephasing diagrams. Finite width laser pulses are used and the calculations are performed for a model spectrum with two or more peaks. Two mechanisms that can result in background and peak suppression are illustrated. The mechanisms are based on differences in homogeneous dephasing times (T_2) or transition dipole matrix element magnitudes. Although the VES line shape differs from the absorption line shape, it is possible to recover the absorption line shape from the VES. The method is demonstrated experimentally on the vibrational mode of CO (center at 1945 cm^{-1}) bound to the active site of the protein myoglobin (Mb-CO). The protein and solvent produce a large absorption background while the VES spectrum of Mb-CO is background free. Calculations are able to reproduce the experimental Mb-CO VES line shape. [S0021-9606(98)01137-4]

I. INTRODUCTION

In this paper, detailed theoretical calculations and the first experimental data using a new ultrafast infrared (IR) pulse technique, vibrational echo spectroscopy (VES) are presented. The VES technique can generate a vibrational spectrum with background suppression using the nonlinear vibrational echo pulse sequence. The vibrational echo is an experimental technique that can extract the vibrational homogeneous line shape even from a massively inhomogeneously broadened vibration line. Recently, vibrational echoes have been applied to the study of liquids, glasses, and proteins.[1–5] VES is a utilization of vibrational echoes to measure spectra rather than dynamics. This technique is one form of two-dimensional vibrational spectroscopy. In this case, the two independently variable parameters are the time delay between the laser pulses and the center frequency of the laser.

Background suppression in VES is in some respects analogous to NMR background suppression techniques.[6,7] In both types of spectroscopy, coherent sequences of pulses are used to remove unwanted spectral features. In the last 50 years, nuclear magnetic resonance and other magnetic resonance spectroscopies have had an enormous impact in the area of molecular structure, chemical dynamics, and biological/medical imaging. The advent of the spin echo, the first NMR coherent pulse technique, in 1950,[8] greatly enhanced the utility of NMR. The spin echo is the precursor of the sophisticated pulse techniques that have been developed subsequently.

Infrared absorption spectroscopy has a much longer history, dating back to Newton's discovery of infrared radiation in the early 1700's. Infrared absorption spectroscopy is a powerful technique for obtaining molecular structural information. In the region of the spectrum conventionally called the midinfrared, there are usually a large number of absorbances, which arise from fundamental, overtone, and combination band transitions. An absorption spectrum provides information about bonding, anharmonicity, solvent interactions, and dynamics. However, even moderate sized molecules can generate spectra with a large number of peaks. For a large molecule, such as a protein, or a solute in a complex solvent, the spectrum may become so crowded that clean observation of the spectral feature of interest can become difficult. In principle, the solvent spectrum can be subtracted out by taking a background spectrum with the solvent alone. However, when the species of interest is in low concentration, accurately performing background subtraction is nontrivial.[9]

In complex molecular systems, such as proteins and other biological molecules, spectral bandwidths tend to be wide compared to the spacing between the bands. The spectral congestion produces broad features, which make structural assignments and quantitative IR absorption spectroscopy measurements difficult.[10,11] There are a number of mathematical techniques that can narrow an absorption line.[12] However, the absorbance width and shape provides information on solute–solvent interactions and, possibly, dy-

[a]Present address: Dept. of Chemistry, Columbia University, New York, NY 10027.
[b]Author to whom correspondence should be addressed. Electronic mail: fayer@fayerlab.stanford.edu

namics, making pure mathematical line narrowing techniques useful but not a perfect solution to the problem of congested spectra.

VES, as detailed below, can reduce or remove unwanted absorption and still return the line position and the line width and shape of the spectral features of interest under certain circumstances. However, because of the relative difficulty of obtaining ultrafast IR pulses, coherent pulsed IR spectroscopy in condensed matter systems is a relatively new field.[13]

There are a number of multiresonant four-wave mixing techniques that have recently been demonstrated including singly or doubly vibrationally enhanced Raman spectroscopy, and vibrationally enhanced infrared spectroscopy[14] VES is a resonant, degenerate, four-wave mixing technique. This technique has the advantage that only a single laser source is needed for the experiments. Further, VES only involves the ground state potential of the molecules of interest. Excitation of electronic modes can significantly perturb the molecules and their interactions with the solvent, possibly adding artifacts to the measured line shape.

In VES, line selectivity can be achieved because nearby transitions can have different homogeneous dephasing times or substantially different transition dipole moments. If the background absorption, which can be a broad, essentially continuous absorption or undesired peaks, has homogeneous dephasing times, T_2^b (where the superscript b indicates background), short compared to the T_2 of the lines of interest, then VES can use the time evolution of the system to discriminate against the unwanted features. The time, τ, between the pulses in the vibrational echo sequence is set such that it is long compared to T_2^b but short compared to T_2. The vibrational echo signal from the background will have decayed to zero while the signal from the desired peaks will be nonzero. Scanning the IR wavelength of the vibrational echo excitation pulses will generate a spectrum in which the background is removed. If the background is composed of a virtual continuum of overtones and combination bands, while the peak of interest is a fundamental, it is likely that $T_2^b < T_2$.

It is also possible to discriminate against the background based on the relative strengths of the transitions even when $T_2^b \cong T_2$. Absorption is proportional to $m\mu^2$ while the echo signal is proportional to $m^2\mu^8$, where m is the concentration of the species and μ is the transition dipole matrix element. If the background is composed of a very high concentration of weak absorbers (m large, μ small) and the spectral features of interest are in low concentration but are strong absorbers (m small, μ large), the background absorption can overwhelm the desired features while the vibrational echo spectrum suppresses the background and enhances the relevant peaks. This situation can occur if the background arises from combination bands and overtones of the solvent while the relevant peaks are low concentration fundamentals. An example like this is presented below where the CO vibrational spectrum of myoglobin-CO (Mb-CO) is examined against a background of the protein and solvent absorptions.

In the following, the basic theory of vibrational echo spectroscopy is outlined in Sec. II. The theory involves calculating the third order nonlinear polarization for laser pulses with finite bandwidths and for a spectrum with several lines. Each spectral line can arise from a species with a particular concentration and transition dipole matrix element and a particular line width determined by the extent of homogeneous and inhomogeneous broadening. In Sec. III, model calculations are presented for two lines that illustrate the conditions for which a broad background or a sharp spectral feature can be suppressed. The relationship between the vibrational echo line shape and the absorption line shape is discussed. In Sec. IV, the experimental procedures used for VES of Mb-CO are briefly outlined, and in Sec. V, the VES of Mb-CO is presented and compared to calculations.

II. VIBRATIONAL ECHO SPECTROSCOPY THEORY

The IR absorption spectrum is related to the two-time correlation function using Fourier transformation:[15–18]

$$I(\omega)=\mathscr{F}[C(\tau)]=\frac{1}{2\pi}\int_{-\infty}^{\infty} dt e^{-i\omega t}\langle \mu(\tau)\cdot\mu^*(0)\rangle, \quad (1)$$

where $\mu(\tau)$ is the transition dipole moment at time τ. The decay of the correlation function arises from both homogeneous and inhomogeneous dephasing. Absorption spectroscopy cannot distinguish between these dephasing mechanisms. The total line shape is the convolution of the homogeneous and inhomogeneous linewidths. The magnitude of absorption as a function of frequency is given by Beer's Law:

$$A(\omega)=\sum_{i,j} \epsilon_{ij}(\omega) m_i l, \quad (2)$$

where $A(\omega)$ is the absorption at frequency ω; $\epsilon_{ij}(\omega)$ is the molar absorbtivity or the extinction coefficient of the jth transition of the ith species. ϵ has units of $M^{-1}\,cm^{-1}$, and is related to the transition dipole matrix element squared.[19] m_i is the concentration of the ith species in the sample, and l is the length of the sample. For the jth transition of the ith species, the absorption is

$$A=\epsilon_{ij} m_i l \propto |\mu^{ij}|^2 m_i l, \quad (3)$$

where μ^{ij} is the transition dipole matrix element of the jth transition of the ith species.

The vibrational echo is an IR time-domain nonlinear technique that removes inhomogeneity from a vibrational line shape. It is the vibrational equivalent of a spin echo in magnetic resonance[8] and a photon echo in electronic excitation spectroscopy.[20,21]

The vibrational echo experiment involves a two pulse excitation sequence. The first pulse excites each solute molecules' vibration into a superposition state, which is a mixture of the $v=0$ and $v=1$ vibrational states. Each vibrational superposition has a microscopic electric dipole associated with it. This dipole oscillates at the vibrational transition frequency. Immediately after the first pulse, all of the microscopic dipoles in the excitation volume oscillate in phase. Because there is an inhomogeneous distribution of vibrational transition frequencies, the dipoles oscillate with some distribution of frequencies. Thus the initial phase relationship is very rapidly lost. This effect is the free induction decay. After a time, τ, a second pulse, traveling along a path making an angle, θ, with that of the first pulse, passes through the sample. This second pulse changes the phase factors of each vibrational superposition state in a manner that initiates a rephasing process. At time 2τ, the ensemble of superposition states is rephased. The phased array of microscopic dipoles behaves as a macroscopic oscillating dipole which generates an additional IR pulse of light, called the vibrational echo. The vibrational echo pulse propagates along a path that makes an angle, 2θ, with that of the first pulse. Subsequently, a free induction decay again destroys the phase relationships, so only a temporally short pulse of light is generated.

The rephasing at 2τ removes the effects of the inhomogeneous broadening.[22] However, fast fluctuations arising from coupling of the vibrational mode of interest to the surrounding environment cause the oscillation frequencies to fluctuate. Thus at 2τ the rephasing is imperfect. As τ is increased, the fluctuations produce increasingly large accumulated phase errors among the microscopic dipoles at 2τ, and the signal amplitude of the vibrational echo is reduced. A measurement of the vibrational echo intensity versus the delay time between the pulses is an echo decay curve. Thus the vibrational echo decay is related to the fluctuations in the vibrational frequencies, not the inhomogeneous spread in frequencies.

The two-pulse vibrational echo, and other line narrowing techniques such as the photon echo,[23] stimulated echo,[24–26] and hole burning,[27–30] eliminate the inhomogeneous contribution to the line shape and are described by four-time correlation functions[31,32,25] of the form:

$$C(t_1,t_2,t_3)=\langle \mu^*(t_3+t_2+t_1)\cdot \mu(t_2+t_1)\cdot \mu(t_1)\cdot \mu^*(0)\rangle, \tag{4}$$

where t_1, t_2, and t_3 refer to three consecutive time intervals. For a vibrational echo, $t_1=t_3=\tau$ and $t_2=0$, so the correlation function simplifies to:

$$C(\tau)=\langle \mu^*(2\tau)\cdot \mu(\tau)\cdot \mu(\tau)\cdot \mu^*(0)\rangle. \tag{5}$$

In many cases, the vibrational echo signal decays as an exponential with the correlation function decaying as

$$C(\tau)=\exp\left(\frac{-2\tau}{T_2}\right), \tag{6}$$

where T_2 is the homogeneous dephasing time. The decay of the correlation function describes the decay of the sample's polarization. The signal in an echo decay experiment is related to the square of the absolute value of the polarization, i.e.,

$$I(\tau)=I(0)\exp\left(\frac{-4\tau}{T_2}\right). \tag{7}$$

(In some circumstances, the vibrational echo decay is not strictly exponential.[33–35])

The correlation function in Eq. (5) is normally written as a trace over three nested commutators of the dipole operator with the density matrix using the Heisenberg representation.[36] This form yields eight terms in the total correlation functions. Two of these terms give rise to the vibrational echo (rephasing echo diagrams) and two others contribute to the signal near $t=0$ (nonrephasing grating diagrams).[37] More details are given below.

The Fourier transform of the four-time dipole correlation function yields the homogeneous line shape

$$I(\omega)=\Im[C(\tau)]=\frac{1}{2\pi}\int_{-\infty}^{\infty} dt e^{-i\omega t}\langle \mu^*(2\tau)\cdot \mu(\tau) \cdot \mu(\tau)\cdot \mu^*(0)\rangle, \tag{8}$$

which for an exponential decay of the correlation function [Eq. (6)] gives a Lorentzian line shape

$$I(\omega)=I_0\,\frac{T_2}{1+(2\pi\Delta\nu)^2T_2^2}. \tag{9}$$

$\Delta\nu$ is the deviation from the center frequency. The Lorentzian line shape will have a FWHM of $1/(\pi T_2)$.[22]

In a standard vibrational echo experiment, the wavelength of the IR light is fixed, and the delay, τ, between the excitation pulses is scanned. In VES, τ is fixed and the wavelength is scanned. In many calculations of electronic state photon echo experiments, and other third order nonlinear experiments, the laser pulse is taken to be a δ function in duration. This greatly simplifies the mathematics, frequently enabling analytical expressions to be obtained for the polarization, and the signal. However, a δ function pulse has an infinite frequency spectrum, and, therefore, the calculated signal is independent of the laser wavelength. To perform the VES calculation it is necessary to use a finite duration pulse, which has a finite bandwidth. The actual shape of the vibrational echo spectrum depends on the bandwidth of the laser pulse and the spectroscopic line shape. Several species with different concentrations, transition dipole moments, line shapes, and homogeneous dephasing times can contribute to the signal. Therefore, VES calculations require determination of the nonlinear polarization using procedures that can accommodate these properties of real systems.

To calculate vibrational echo spectra, i.e., the vibrational echo intensity as a function of laser wavelength, including the details of the sample and laser pulses used in a real experiment, an efficient numerical algorithm for computing the vibrational echo signal for laser pulses of finite duration is employed.[38] In the experiment presented below, the pulse shapes are Gaussian, so the problem is considered for Gaussian pulses although the calculations can be performed for other pulse shapes. The spectrum is calculated by numerically evaluating all of the terms for the third order nonlinear polarization that contribute to the signal in the vibrational echo geometry.[38]

In Eq. (10) below, in general, there are three independent fields, which may have differing spectral and temporal envelopes. However, experimentally, a vibrational echo is performed using pulses that are split from a parent pulse. In this situation, the applied frequency for each field is identical and the temporal envelopes only differ by a time shift, t. The four contributions to the polarization necessary to calculate the signal in the vibrational echo phase matched direction for a

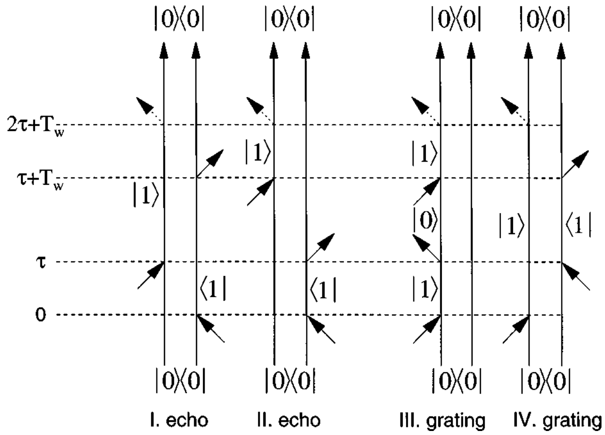

FIG. 1. Double sided Feynman diagrams for all contributions to a two pulse four-wave mixing experiment in the $\vec{k}_s = 2\vec{k}_2 - \vec{k}_1$ direction. The two vertical lines represent the ket and the bra of the density matrix. Time increases from bottom to top. The arrows indicate interaction with the electromagnetic field from the corresponding pulse. To the left of the diagrams, the pulse sequence timing is shown. In the vibrational echo, the second and third interaction are in the second optical pulse so T_w corresponds to the time between two electric field interactions in the same pulse. Diagrams I and II contribute to the true vibrational echo signal in that they are responsible for rephasing of inhomogeneous broadening. For slow homogeneous dephasing, they contribute to the signal at times long compared to zero delay time, $t=0$. Diagrams III and IV only contribute to the polarization near $t=0$.

two level system are shown in Fig. 1. As an example, the expression for one term of $P^{(3)}$ arising from the diagram denoted I in Fig. 1 is given by

$$P_1^{(3)} = \left(\frac{1}{i\hbar}\right)^3 m\rho_{aa}(0)\mu_{ab}\mu_{ba}\mu_{ab}\mu_{ba}E^*_{\mathbf{k}_1}E^2_{\mathbf{k}_2}\exp(i\mathbf{k}_s\cdot\mathbf{r})$$
$$\times\int_{-\infty}^{t_s} dt_3 G_{ba}(t_s-t_3)\{\xi_{\mathbf{k}_2}(t_3-\tau)\exp[-i\omega_l(t_3-\tau)]\}$$
$$\times\int_{-\infty}^{t_3} dt_2 G_{bb}(t_3-t_2)\{\xi_{\mathbf{k}_2}(t_2-\tau)$$
$$\times\exp[-i\omega_l(t_2-\tau)]\}\int_{-\infty}^{t_2} dt_1 G_{ab}(t_2-t_1)$$
$$\times[\xi_{\mathbf{k}_1}(t_1)\exp(i\omega_l t_1)]. \tag{10}$$

$\rho_{aa}(0)$ is the initial density matrix element for this quantum pathway, I; μ_{ab} is the transition dipole moment between states a and b; $\exp(i\mathbf{k}_s\cdot\mathbf{r})$ describes the spatial characteristics of the generated polarization; and $G_{ab}(t''-t')$ is the Liouville propagator that describes the evolution of the density matrix element ρ_{ab} between times t'' and t'. The laser pulses are Gaussian wave packets with $E_{\mathbf{k}_i}$, a complex coefficient describing the maximum electric field of the plane wave along wave vector $\mathbf{k}_i$, $\xi_{\mathbf{k}}(t')$, the slowly varying Gaussian envelope of the laser pulse taken to be a plane wave with wave vector, $\mathbf{k}_i$, and $\exp(i\omega_l t')$, the high frequency component of the wave packet's electromagnetic field along $\mathbf{k}_i$ with frequency ω_l, where ω_l is the laser frequency.

In standard treatments of the third order polarization,[39] the density matrix is taken to have a trace of 1. Actually, the calculations are always for an ensemble of N molecules contained in the volume in which the radiation fields interact with the material. Therefore, the trace of density matrix should be N. For most purposes, this does not matter since it is the time dependence that is of interest and not the strength of the signal. The number of molecules per unit interaction volume, N/V, is a number density or concentration. In the context of VES, the relative concentrations of various species play an important role. Therefore, in Eq. (10), the trace of density matrix is taken to be 1, but a concentration, m, is explicitly included. Note that the third order polarization is proportional to the fourth power of the transition dipole matrix element, μ^4, and is linear in the concentration, m, of the species that interacts with the fields.

Diagrams I, II, III, and IV in Fig. 1 show the time ordered quantum pathways which contribute to the third order nonlinear polarization, $P^{(3)}$, in the vibrational echo phase matched direction, $\mathbf{k}_s = 2\mathbf{k}_2 - \mathbf{k}_1$, for a two level system where the applied field at frequency ω_l is resonant (within the laser pulse bandwidth) with the transition frequency ω_{ab}. Diagrams I and II have time ordered interactions which correspond with the time ordering of the applied pulse sequence and are responsible for the true vibrational echo, i.e., rephasing of the inhomogeneous broadening. Diagrams III and IV have time ordered interactions which do not correspond to the ordering of the pulse sequence. These diagrams only contribute to a nonzero $P^{(3)}$ when the delay between the first and second pulses is short enough such that the electric field envelopes overlap. These diagrams only contribute to the signal around zero time delay between the pulses.[40]

Frequently, the contributions from diagrams III and IV are not included in describing echo decay experiments because the damping of the material response is slow compared to the pulse duration. The information in the experiment is present in the decay, which extends many pulse durations after the rising edge of the vibrational echo response. However, in echo decay experiments in which T_2 is comparable to the pulse duration, proper analysis of the decay requires inclusion of diagrams III and IV.[2,3,5] In the current application, theory is used to calculate the vibrational echo spectrum. VES is possible even when T_2 is fast compared to the laser pulses since it is possible to have zero pulse delay, scan the laser wavelength, and record the spectrum. Therefore, it is necessary to include all four diagrams in the calculations.

For a single transition of one species, the total third order polarization is the sum of the third order polarizations from each of the four diagrams shown in Fig. 1:

$$P_{\text{tot}}^{(3)} = \sum_{N=1}^{IV} P_N^{(3)}. \tag{11}$$

To calculate the vibrational echo observable for a fixed laser frequency, ω_l, $P^{(3)}$ must be integrated over the inhomogeneous line, $g(\omega_{ba})$ and then the modulus square of the result must be integrated over all time since the observable is the integrated intensity of the echo pulse,

$$I_s(\tau,\omega_l) \propto \int_{-\infty}^{\infty} dt_s \left| \int_0^{\infty} d\omega_{ba} g(\omega_{ba}) P_{\text{tot}}^{(3)}(\omega_{ba}, t_s, \omega_l) \right|^2. \tag{12}$$

τ is the separation between the two laser pulses. The numerical calculation of the vibrational echo spectrum with realistic laser pulse envelopes and realistic material properties involves a five-dimensional integral. This is the situation for a single transition of a single species. In general, there are two or more spectroscopic lines with independent $P^{(3)}$. The contribution from each transition of each species must be summed at the polarization level

$$I_s(\tau,\omega_l)\propto\int_{-\infty}^{\infty}dt_s\left|\sum_{i,j}\left[\int_0^{\infty}d\omega_{ab}^{i,j}g_{i,j}(\omega_{ab}^{i,j})\times P_{\mathrm{tot},i,j}^{(3)}(\omega_{ab}^{i,j},t_s,\omega_l)\right]\right|^2, \quad (13)$$

where i is the label for the species and j is the label for the jth transition of the ith species. It is necessary to distinguish between transitions on different species since the species may have different concentrations as well as the transitions having distinct line shapes, $g_{i,j}(\omega_{ab}^{i,j})$, and transition dipole matrix elements, $\mu_{ab}^{i,j}$.

In the calculations that are presented below, the laser pulse shapes and the inhomogeneous line shapes are Gaussian. The homogeneous line shapes are Lorentzians.

III. MODEL CALCULATIONS

In this section a variety of model calculation are presented to illustrate various features of VES. The calculations are performed using Eq. (13). Comparisons are made to corresponding calculated absorption spectra. The calculations demonstrate peak and background suppression using VES. Suppression based on differences in transition dipole matrix elements and based on differences in T_2 are both illustrated. While the VES line shape is not the same as that obtained from an absorption spectrum, it is shown that it is possible to recover the absorption line shape from a vibrational echo spectrum. In Sec. V, the same calculation procedures are applied to the experimental vibrational echo spectrum of the CO stretching mode of myoglobin-CO.

Figure 2 displays calculated absorption spectra and vibrational echo spectra. The calculations are for a hypothetical solvent/solute system in which there is a low concentration strongly absorbing solute and a high concentration weakly absorbing solvent. Figure 2A displays the absorption spectra of the solvent and solute. The peak centered at 2000 cm^{-1} is from the solvent which has a relative concentration of unity and a relative transition dipole moment of unity. The peak centered at 1900 cm^{-1} is from the solute which has a relative concentration of 10^{-4} and has a relative transition dipole moment of 100. Thus the two peaks have the same absorbance [see Eq. (3)]. The vibrational echo spectra are shown in the Fig. 2B and 2C. The calculations were performed for the delay time $\tau=0$. Both peaks are taken to have 15 cm^{-1} and 1 cm^{-1} inhomogeneous and homogeneous linewidths, respectively. The laser pulse bandwidth is 1 cm^{-1}. In Fig. 2B, the vibrational echo spectrum of the solute is large while that of the solute is undetectable. In Fig. 2C, the calculation shown in 2B has been multiplied by a factor of 10^8. The spectrum of the solvent is now visible. For the parameters used, the vibrational echo spectrum of the solvent is reduced 10^8 relative to that of the solute. As can be seen in Eq. (10), the vibrational echo polarization depends on the transition dipole matrix element to the forth power, μ^4, and it is linear in the concentration, $m\propto\rho(0)$. At the signal level, the vibrational echo signal is proportional to $m^2\mu^8$ for each species while the absorption spectrum is proportional to $m\mu^2$. For the solute m is 10^{-4} while μ is 10^2 relative to the solvent. While the solute and solvent optical densities are identical, the solute vibrational echo spectrum is 10^8 greater in magnitude then the solvent spectrum.

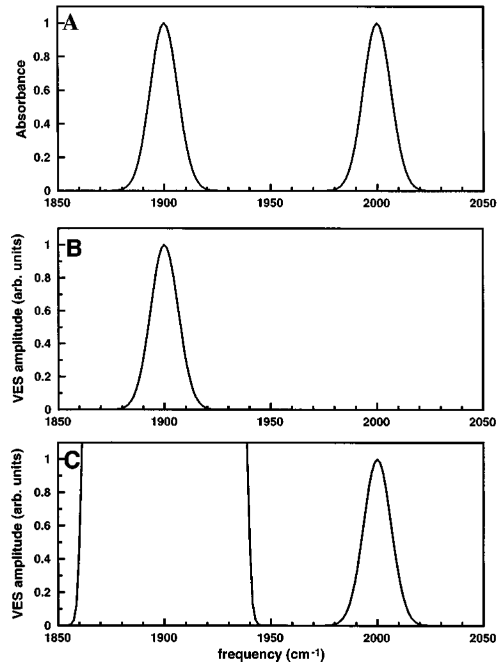

FIG. 2. Illustration of VES peak suppression. The system consists of a peak at 1900 cm^{-1} and one at 2000 cm^{-1}, both with an absorbance of 1. The peak at 2000 cm^{-1} arises from a hypothetical concentration and transition dipole matrix element such that the total absorbance is 1. The peak at 1900 cm^{-1} arises from a concentration reduced by 10^{-4} and transition dipole increased by 100 relative to the other peak, also yielding an absorbance of 1. (A) The calculated absorption spectrum. (B) The calculated VES spectrum. The high concentration, small transition dipole moment peak is suppressed. (C) A 10^8 magnification of (B) shows the echo signal of the suppressed peak.

Figure 3 displays model calculations for a system with a broad strong solvent absorption and a narrow weak solute absorption. The abscissa is centered about the peak of the solute spectrum. Figure 3A is an absorption spectrum. The parameters have been selected so that the broad solute absorption is 100 times stronger than the solute absorption. The inset shows a magnified view of the solute absorption. Figures 3B and C show background free vibrational echo spectra demonstrating two mechanisms of solvent background suppression. In Fig. 3B the spectrum is taken with $\tau=0$, and the suppression occurs because the solute has a large μ but small concentration relative to the solvent. This is analogous to the peak suppression shown in Fig. 2. The suppression occurs because of the $m^2\mu^8$ dependence of the vibrational echo spectrum versus the $m\mu^2$ dependence of the absorption spectrum. This situation may be encountered in real systems in which the peak of interest is a solute fundamental while the background consists of overtones and combination bands

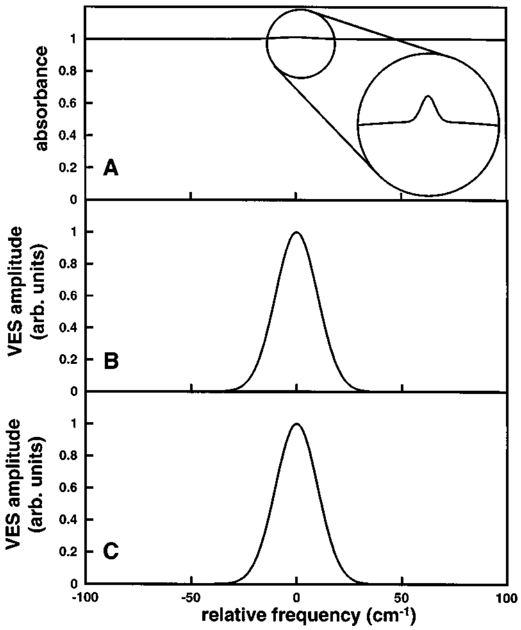

FIG. 3. Figure 3 displays model calculations for a system with a broad strong solvent absorption and a narrow weak solute absorption. The abscissa is centered about the peak of the solute spectrum. (A) is the absorption spectrum. The parameters have been selected so that the broad solvent absorption is 100 times stronger than the solute absorption. The inset shows a magnified view of the solute absorption. (B) and (C) show background free vibrational echo spectra demonstrating two mechanisms of solvent background suppression. In (B) the spectrum is taken with $\tau=0$, and the suppression occurs because the solute has a large μ but small concentration relative to the solvent. (C) is an example of T_2 suppression. The solute and solvent μ and m were selected to give similar vibrational echo signals at $\tau=0$. However, in this case, the solute $T_2=10$ ps and the solvent $T_2=1$ ps. The pulse delay is $\tau=5$ ps. Because T_2 for the solvent is fast and T_2 for the solute is slow, it is possible to select a delay time at which the solvent vibrational echo spectrum is eliminated while the solute vibrational echo spectrum is still significant.

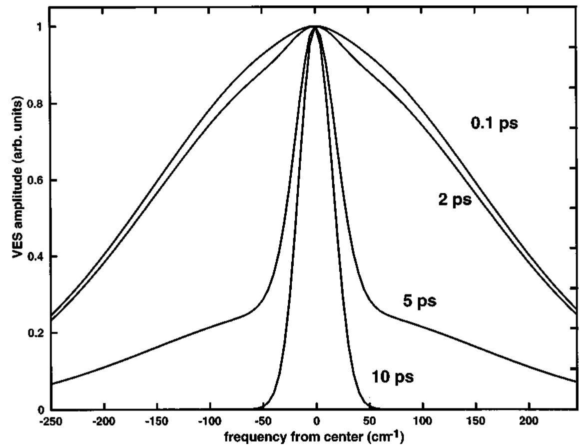

FIG. 4. Calculations to illustrate T_2 contrast. The system is two Gaussians. The ''solvent'' Gaussian has an amplitude of 1, an inhomogeneous width of 500 cm^{-1} and a T_2 of 0.1 ps. The ''chromophore'' Gaussian has an amplitude of 0.01, an inhomogeneous width of 50 cm^{-1} and a T_2 of 1.0 ps. The center frequencies of both are the same. The lines illustrate a variety of delays between the two echo pulses. At a delay of 0.1 ps, the VES shows the massive solvent peak with a barely visible contribution from the chromophore. By extending the delay to 2 ps and 5 ps, the solvent contribution becomes less and less significant. At 10 ps, the solvent contribution is gone and only the chromophore VES is visible. Spectra are normalized.

of the solvent. This is the situation in the experiments presented in Sec. V.

Figure 3C is an example of T_2 suppression. The solute and solvent μ and m were selected to give similar vibrational echo signals at $\tau=0$. However, in this case, the solute $T_2=10$ ps and the solvent $T_2=1$ ps. The pulse delay is $\tau=5$ ps. Because T_2 for the solvent is fast and T_2 for the solute is slow, it is possible to select a delay time at which the solvent vibrational echo decay is essentially complete while the solute vibrational echo signal is still significant [see Eq. (7)]. The result is background suppression based on the dynamics of the system rather than on the static properties of m and μ. If the peak of interest is a fundamental of the solute while the background is basically a continuum of overtone and combination bands of the solvent, T_2 suppression can be viable. T_2 suppression of the background is equivalent to T_2 image enhancement in magnetic resonance imaging.

Figure 4 illustrates the nature of T_2 suppression by presenting vibrational echo spectra for two spectral lines with different T_2's as a function of delay time. One of the lines has a very short $T_2=1$ ps and a broad inhomogeneous linewidth. This broad line contributes the vast majority of the signal (99.9%) at $\tau=0$ because of the values used for the parameters, μ and m. The other line has a significantly longer $T_2=10$ ps and a narrower inhomogeneous linewidth. For both absorption bands, the inhomogeneous linewidths are large compared to the homogeneous linewidths. In a manner similar to Fig. 3, an absorption spectrum would show only the broad line. The four curves displayed in Fig. 4 are vibrational echo spectra calculated for four different delay times, τ. Each of the four curves has been scaled so that it has the same height at line center although the maximum magnitude of the spectrum decreases as τ increases. Curve A is the calculated vibrational echo spectrum at $\tau=0.1$ ps. The spectrum is essentially the spectrum of the fast T_2 line. Curve B is calculated with $\tau=2$ ps. The influence of the slower T_2 line is becoming visible. At this delay time, the polarization generated by the fast T_2 line has dropped while the polarization generated by the slow T_2 line is almost unchanged. In curve C ($\tau=5$ ps), the signal from the fast T_2 line is smaller than that of the slow T_2 line. Finally, in curve D ($\tau=10$ ps), the polarization produced by fast T_2 line is virtually zero. While the vibrational echo signal from the slow T_2 line is reduced, this narrow inhomogeneous line now totally dominates the spectrum. This is an ideal example in which the differences in T_2 are large enough that the unwanted line can be completely suppressed. If the T_2's are not too different, a spectrum such as curve C may be produced. The buried line is revealed and the background is partially suppressed. Considerable information can be extracted from such a spectrum. As discussed below, it is possible to determine the absorption line shape from VES data.

As in any spectroscopic technique, VES has an instrument resolution function. If this is small compared to the vibrational linewidth, the vibrational echo spectrum at the polarization level is identical to the absorption spectrum. Since the signal is detected at the intensity level, the vibration echo spectrum is the square of the absorption spectrum

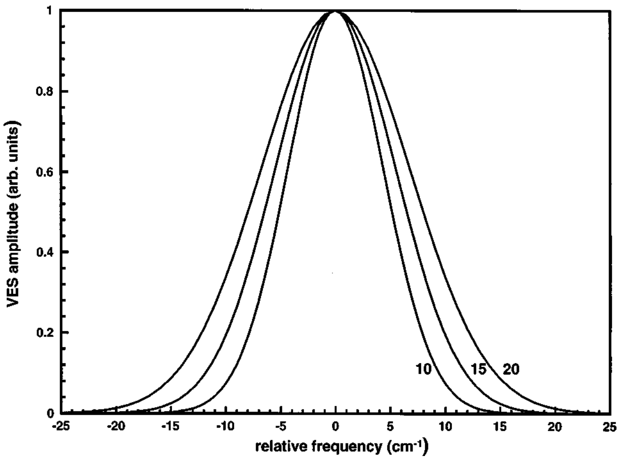

FIG. 5. Inhomogeneous linewidth dependence. VES calculations using fixed laser bandwidth of 1 cm^{-1} and fixed homogeneous line width of 15 cm^{-1}. The lines represent spectra for various inhomogeneous linewidths. This example illustrates that small differences in the line width can be seen. The VES can be fit, and the absorption spectrum can be recovered.

(see comment on inner filter effect below). In Fig. 2, it can be seen that the echo spectrum in panel B is narrower than the absorption spectrum in panel A. Figure 5 illustrates the sensitivity of the vibrational echo spectrum to changes in width. The instrument resolution function is determined by the laser bandwidth. For the examples in Fig. 5, the bandwidth is 1 cm^{-1} while the absorption linewidths are more than 10 times greater. In this case, the instrument function is negligible. The calculated curves in Fig. 5 are the square of Voight profiles, i.e., the square of the convolution of a Gaussian inhomogeneous line with a Lorentzian homogeneous line. In each calculation, the Lorentzian width is fixed at 15 cm^{-1} while the Gaussian width is varied from 10 cm^{-1} to 20 cm^{-1}. As the inhomogeneous width broadens, the vibrational echo spectrum broadens. The increase in width is less than the 5 cm^{-1} increment because of the relatively large, fixed homogeneous contribution. Nonetheless, the change in the calculated vibrational echo spectrum is clearly discernible. To determine the absorption line shape for an experimental situation like the one depicted in Fig. 5, the line shape is fit to the square of a Voight profile. Once a satisfactory fit is achieved, the absorption spectrum is the Voight used to obtained the fit. However, as in any spectroscopy, if the laser bandwidth is comparable to the spectral width, the VES will be broadened. In this case, the VES calculation can be performed using the known characteristics of the laser spectrum and varying the input absorption spectrum until a fit to the data is achieved.

In most situations in which VES might be used, the vibrational echo spectrum is related to the absorption spectrum as described above. However, there is another factor that can influence the shape of the vibrational echo spectrum, i.e., the inner filter effect on nonlinear spectroscopy.[38] Consider the type of spectrum displayed in Fig. 2. If the peak of the absorption spectrum has a large absorbance, then the input pulses and the out going vibrational echo signal will be significantly attenuated at the peak of the spectrum but not in the wings. This will make the signal artificially small at the peak compared to the wings. The result is broadening of the spectrum and a change in shape. It is possible to calculate a correction for the inner filter effect. The result is given in Eq. (14) below, and the derivation is given in the Appendix. In some situations, the desired spectrum is a small contribution to a large background, e.g., see Fig. 3. In this case, the spectral feature of interest contributes little to the over all absorption. The shape of the vibrational echo spectrum is not changed as long as the background does not change absorbance substantially across the wavelength range of interest. This is the situation shown below for Mb-CO.

IV. EXPERIMENTAL PROCEDURES

VES requires a tunable source of infrared pulses. These can be provided by conventional laser systems using optical parametric amplifiers to down convert visible or near-IR light into the mid-IR or far-IR region necessary to perform vibrational spectroscopy. In the experiments presented below on Mb-CO, vibrational echo decays[2] and vibrational echo spectra were taken with the stanford free electron laser (FEL).[3]

The experiments described below were performed using infrared pulses near ~5 μm. The FEL generates nearly transform limited pulses with a pulse duration that is adjustable between 0.7 ps and 2 ps. Active frequency stabilization allows wavelength drifts to be limited to <0.2 cm^{-1}. The pulse duration and spectrum were monitored continuously with an autocorrelator and a grating monochromator, respectively. The FEL produces a ~2 ms macropulse at a ~5 Hz repetition rate. Each macropulse consists of the ps micropulses at a repetition rate of 11.8 MHz (84.7 ns). The micropulse energy at the input to experimental optics is 0.5–1.0 μJ.

In vibrational experiments, virtually all power absorbed by the sample is deposited as heat. To avoid sample heating problems, micropulses are selected out of each macropulse at a repetition rate of 25–60 kHz by Ge acousto-optic modulator single pulse selectors. This pulse selection yields an effective experimental repetition rate of ~1 kHz, and an average power <0.5 mW.

The two pulses for the VES experiment were obtained using a 10%R beam splitter. The 10% beam is single pulse selected using an Ge AOM and sent through a computer-controlled stepper motor delay line. The remaining portion (second pulse in the vibrational echo pulse sequence) is single pulse selected by a second Ge AOM. The first AOM selects pulses at 25 kHz, i.e., half the rate of the second pulse, permitting subtraction of scattered light background generated by the stronger pulse that is also spatially closer to the vibrational echo signal. The two pulses were focused in the sample to ~50 μm diameter spots using an off-axis parabolic reflector for achromatic focusing of the IR. The vibrational echo signals are measured with an InSb detector, gated integrators, and digitized for collection by computer.

Careful studies of power dependence and repetition rate dependence of the data were performed. It was determined that there were no heating or other unwanted effects when vibrational echo experiments were performed with pulse energies of ~200 nJ and an effective repetition rate of 1 kHz (50 kHz during each macropulse).

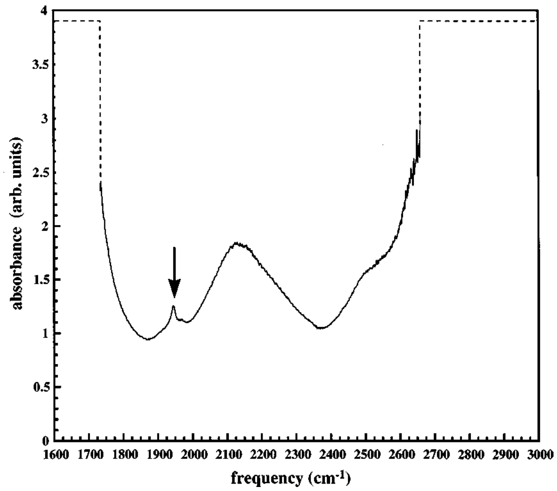

FIG. 6. Fourier transform infrared spectrum of Mb-CO. The A_1 CO mode is indicated with an arrow. The CO mode is on top of a broad background of high concentration, low absorbing species. Because of the high protein concentration, the light at frequencies above 2700 cm^{-1} and below 1600 cm^{-1} is completely absorbed.

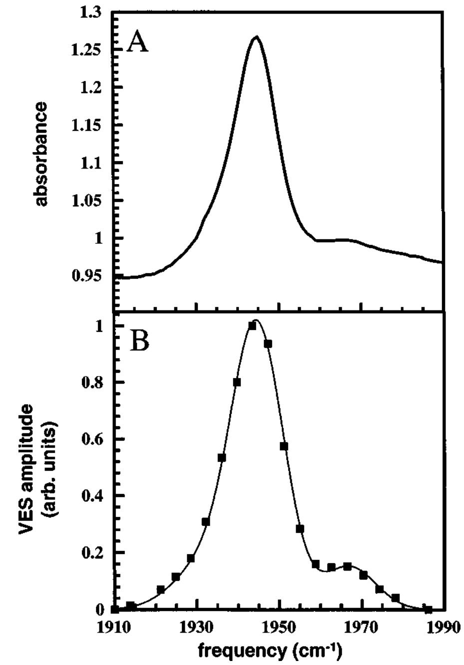

FIG. 7. Example of data and comparison to theory and spectrum. (A) The Mb-CO absorption spectrum, a magnification of data shown in Fig. 6. Note that the background (protein and solvent) have an absorbance of ~0.95. The A_1 peak has an absorption of about 0.3 above this background. (B) The square root of the experimental vibrational echo intensities at a fixed pulse delay with the laser wavelength varied (squares). The VES gives a line shape wider than the absorbance spectrum. The solid line is a calculated VES using known parameters (see text for details). The important feature of the VES is that it reproduces the spectrum with zero background.

In the data presented here, VES measurements were made at a number of fixed frequency points rather than continuously scanning the FEL. The data collection at fixed points was necessary because of the configuration of the FEL. It is possible to scan the FEL continuously, and it is also possible to scan OPA based systems continuously. In recent VES experiments, currently under investigation, we have been able to perform the VES experiment while scanning the FEL. This advance has greatly increased our frequency resolution and decreased our experimental time. These details will be published subsequently.[41]

V. EXPERIMENTAL RESULTS

The first VES experiments were conducted on CO bound to myoglobin in 22 mol% ethylene glycol:water at 280 K. Myoglobin is a protein used in the storage and transport of O_2 in muscle tissues. In this system, another biologically relevant ligand, CO is bound at the active site of this protein. There have been a number of detailed vibrational echo decay studies of this Mb-CO system and similar systems.[2,3,42,43] Conformational variations in the protein structure result in the CO stretching mode having three bands, labeled $A_0(\sim 1969\ \mathrm{cm}^{-1})$, $A_1(\sim 1945\ \mathrm{cm}^{-1})$, and A_3 $(\sim 1930\ \mathrm{cm}^{-1})$ in decreasing frequency.[44] Many external parameters, such as temperature, pH, and solvent viscosity can sig-nificantly change the relative populations of the three conformations.[44,45]

Figure 6 displays the absorption spectrum of Mb-CO. The Mb-CO spectrum is a small feature at ~1950 cm^{-1} on top of a background with absorbance ~1. The background is composed of absorption by both the protein and the solvent. To obtain a CO spectrum that is clearly visible above the background, it is necessary to prepare a sample with a high concentration of protein (15–20 mM) in a short path length cell (200 μm) to reduce the contribution to the background from the solvent. Since there is one CO per protein molecule, the background arising from the protein cannot be reduced. At frequencies above ~2700 cm^{-1} and below 1600 cm^{-1}, the sample absorbs essentially all of the light. Figure 7(A) displays an expanded view of the region of the Mb-CO spectrum. The A_1 peak is the largest peak with the A_0 peak discernible at ~1969 cm^{-1}. A_3 is a shoulder on the red side of A_1.[44,45] The A_1 peak has an absorbance of ~0.3 above the background.

Figure 7(B) displays VES data (squares) for Mb-CO along with a theoretical calculation of the vibrational echo spectrum. As discussed in Sec. IV, the spectrum was taken point by point because the FEL could not be continuously scanned in the configuration used for these experiments. The amplitude of each point was determined from the magnitude of the vibrational echo signal at a fixed delay τ. Figure 7(A) displays an expanded view of the Mb-CO absorption spectrum scaled to facilitate direct comparison to the VES data. Note that the absorption axis in Fig. 7(A) begins at 0.90. The VES data points in Fig. 7(B) display the square roots of the VES signal at a range of frequencies ($\Delta\lambda = 0.01\ \mu$m) at $\tau = 0$. As the laser wavelength is changed, there is some change in the pulse intensity. This change in intensity with wavelength will effect the magnitude of the signal. Therefore, the signal was normalized to the laser intensity. The VES signal is proportional to I_0^3, where I_0 is the input intensity if the sample is optically thin. This is also the appropriate normalization factor if the sample is not optically thin but the absorbance does not change with wavelength over the spectral range of interest. Figure 7(B) shows the square root of the VES data with I_0^3 normalization.

For a sample which is not optically thin and there is a substantial wavelength dependence of the absorbance, a more detailed normalization factor is required. Each wavelength is normalized by a factor $N(\omega)$, which has the form

$$N(\omega)=I_0^3(\omega)\exp(-A(\omega))\left\{\frac{[1-\exp(-A(\omega))]}{A(\omega)}\right\}^2, \quad (14)$$

where $A(\omega)$ is the sample's wavelength dependent absorbance. The correction factor for this inner filter effect can be obtained using a conventional IR absorbance spectrum and a measurement of the wavelength dependence of the relative input intensity, I_0. The derivation of Eq. (14) is presented in the Appendix. Equation (14) applies for the laser bandwidths that are small compared to the wavelength differences over which the absorbance changes significantly. It can be generalized for situations in which the laser bandwidth is large compared to the wavelength difference. For the Mb-CO sample, the background is fairly flat and the peak is small compared to the background. Therefore, corrections for the inner filter effect are not large, and they have not been included in the analysis.

In Fig. 7(B), the square root of the vibrational echo spectrum is presented because it is more closely related to the absorption spectrum. As discussed above, the vibrational echo spectrum at the polarization level is directly related to the absorption spectrum. The height of the spectrum has been scaled to 1. Unlike the absorption spectrum in Fig. 7(A), the vibrational echo spectrum has zero background. The protein and solvent do not contribute to the vibrational echo spectrum in the vicinity of 1950 cm^{-1} although they dominate the absorption spectrum (see Fig. 6). The vibrational echo spectrum displays no background even with $\tau=0$. This indicates that the selectivity arises from differences in transition moments rather than in T_2s (see Fig. 2 and the surrounding discussion). However, even at $\tau=0$, a difference in T_2's will contribute to background suppression if the pulses are significantly longer than the background T_2 but comparable to or longer than the T_2 of the peaks of interest. The width of the vibrational echo spectrum in Fig. 7(B) is somewhat wider than the absorption spectrum because the bandwidth of the laser (13 cm^{-1}) is comparable to the spectral linewidth.

The solid line in Fig. 7(B) is the calculated vibrational echo spectrum using the procedures outlined in Sec. II. The spectrum was modeled as having three independent transitions at different center frequencies but with the same homogeneous widths, inhomogeneous widths, and transition dipole moments as the A_1 state. The homogeneous width was determined using a vibrational echo decay. The echo decay experiments show that the linewidth arises predominantly from inhomogeneous broadening. The absorption linewidth of the A_1 peak was determined from spectra. There is some uncertainty in this width because of the overlapping lines and the large background absorption. The center frequencies of the three transition are those reported in the literature[44,46] and given above. The pulse duration, spectral width, and shape of the laser pulses are known from autocorrelations and spectra. The only adjustable parameters used were the relative amplitudes of the three lines. Since the transition moments are the same, the relative amplitudes are determined by the relative populations (concentrations) of the three structural states. In the calculation displayed in Fig. 7(B), the relative populations of the A_0, A_1, and A_3 modes are ~3%, ~95%, and ~2%, respectively. Like the data, the solid line is the square root of the calculated vibrational echo spectrum. As can be seen, the calculation matches the experimental results quite well. While the A_3 line is not visible as a distinct peak, it was found that without including it in the calculation, the high energy side of the calculated spectrum fell off much faster than the data.

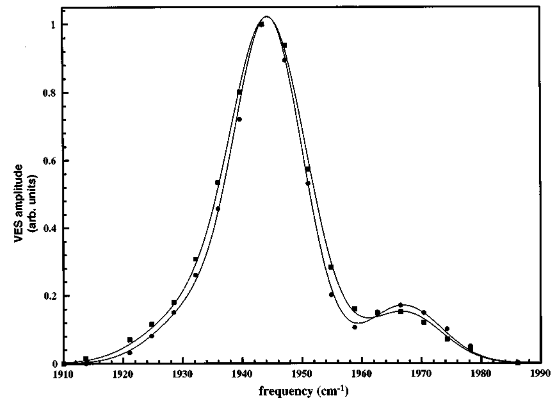

FIG. 8. VES spectra at two pulse delays. The squares are the same data shown in Fig. 7 which are for zero delay. The circles are for the same sample but at a delay between the pulses of 2.5 ps. The spectrum is normalized because the absolute size of the VES spectrum is smaller at longer delay. The A_0 mode (peak at 1966 cm^{-1}) is enhanced relative to the A_1 mode (peak at 1945 cm^{-1}) because the A_0 mode has a slightly (~20%) longer T_2 than that of the A_1.

The important point demonstrated by Fig. 7(B) is that the theoretical development outline in Sec. II can reproduce the VES data. In this case, information from the absorption spectrum was used to show that the VES data could be reproduced. The utility of VES will be in situations where the absorption spectrum is not available. The close agreement between the data and the calculations indicate that the method can be used to extract reliable spectroscopic information.

Figure 8 shows the VES data at two delay times, τ. The zero delay is the same data shown in Fig. 7(B). The 2 ps delay data are a mild demonstration of the type of T_2 peak selectivity shown in theoretical curves in Fig. 2. The VES spectra were normalized at the A_1 center peak. As can be seen from the data, the other conformer dephasing times are different than that of the A_1 conformer. While the difference is small, the A_0 peak is clearly enhanced relative to the A_1 peak at the longer delay. This indicates that the dephasing time of the A_0 mode is slower than that of the A_1.

VI. CONCLUDING REMARKS

Vibrational echo spectroscopy was described theoretically and illustrated with experiments on the vibrational stretching mode of CO bound to the active site of the protein, myoglobin. VES employs the vibrational echo pulse sequence to take vibrational spectra rather than the normal application of ultrafast IR vibrational echoes, the study of vibrational homogeneous dephasing dynamics in condensed phases. The theory and experiments demonstrate that VES has the ability to suppress a broad, highly absorbing background to enhance the spectrum of the peaks of interest. The suppression can occur either through transition dipole moment selectivity or through homogeneous T_2 selectivity. It is also possible to accentuate certain spectral lines over others under the right circumstances. In some respects, VES is akin to techniques commonly used in NMR, which are absent in conventional vibrational spectroscopy. VES uses a coherent pulse sequence to take a spectrum while eliminating unwanted aspects of the spectrum. The technique is most like NMR when T_2 selectivity is used to change the relative amplitude of spectral peaks. In this application, VES is a type of two-dimensional vibrational spectroscopy. The two dimensions are frequency and the time, τ, in the echo pulse sequence.

In the experiments, the vibrational echo spectrum was taken point-by-point because of the nature of the free electron laser used to do the experiments. It is possible for the FEL to be configured to scan continuously. Therefore, spectra could be taken in a more conventional manner. It is not necessary to use a FEL to perform VES experiments. IR can be generated using optical parametric amplifiers pumped by conventional lasers. Commercial IR OPAs are available that can be pumped by commercial laser systems. Therefore, VES can be performed with commercial table top laser systems.

Ultrafast infrared vibrational echo experiments and VES are initial steps in the development of coherent vibrational spectroscopy of complex condensed matter molecular systems. As ultrafast IR sources become more available, the use of coherent IR pulse sequence spectroscopic techniques will become increasingly important tools in the study of complex molecular systems.

ACKNOWLEDGMENTS

We would like to thank Professor Dana D. Dlott, Department of Chemistry, University of Illinois at Urbana-Champaign for many useful discussions regarding this work. We would also like to thank Professors Alan Schwettman and Todd Smith, Department of Physics, Stanford University, and their research groups, especially Dr. Chris Rella, at the Stanford Free Electron Laser Center whose efforts made these experiments possible. This research was supported by the Office of Naval Research, (N00014-94-1-1024), by the National Science Foundation, Division of Materials Research (DMR-9610326), and by the Office of Naval Research, (N00014-92-J-1227-P00006).

APPENDIX: THE INNER FILTER NORMALIZATION

This Appendix shows the derivation of Eq. (14), the correction for the inner filter effect. Consistent with the perturbation treatment used in the derivations of the VES, the experiment is assumed to be conducted in the low power limit. Therefore, the polarization generated by the sample is negligible compared to the electric field of the excitation pulses and does not contribute to field seen by the molecular vibrations. The absorbance is assumed to not change significantly across the laser bandwidth. The treatment can be generalized to laser bandwidths that are large compared to wavelength differences on which significant changes in absorbance occur.

Consider a sample with thickness L that is divided into N slices. Beer's law shows that the electric field transmission through a slice of length l is

$$E=E_0 \exp\left(-\frac{\epsilon m l}{2}\right), \tag{A1}$$

where E_0 is the input electric field, ϵ is the extinction coefficient, m is the concentration, and l is the path length. While there may be several species of varying extinction coefficients and concentrations contribution to the absorption, only the product $\alpha=\epsilon m$ matters. The first slice of the sample generates a polarization at the back of the first slice proportional to

$$P(l)=\gamma E_0^3 \exp\left(-\frac{\alpha L}{2}\right). \tag{A2}$$

The polarization is related to E_0^3 because there are three interactions with the field in the vibrational echo experiment, as detailed above. The exponential term is the attenuation of the signal as it passes through the rest of the sample. γ contains all other factors influencing the polarization such as the concentration and transition dipole matrix element of the molecular oscillator giving rise to the echo signal.

The contribution to the polarization at the back of the sample from the ith slice is

$$P(i)=\gamma\left[E_0 \exp\left(-\frac{\alpha i l}{2N}\right)\right]^3 \exp\left(\frac{-\alpha(N-i)l}{2N}\right). \tag{A3}$$

The first term in brackets is the electric field, attenuated by passage through i slices, cubed. The second term is the attenuation of the polarization generated in the ith slice as it passes through the subsequent $N-i$ slices. $Nl=L$, the sample thickness. The total signal at the back of the sample is the absolute value squared of the sum of the polarization from each slice at the back of the sample,

$$S=\left|\sum_{i=1}^{N} P(i)\right|^2=\left|\sum_{i=1}^{N} \gamma\left[E_0 \exp\left(-\frac{\alpha i l}{2N}\right)\right]^3 \times\exp\left(-\frac{\alpha(N-i)l}{2N}\right)\Big/ N\right|^2. \tag{A4}$$

The N in the denominator is a normalization factor that prevents the signal from growing as the number of slices in the sum is increased. For the beam propagation direction along the x axis, taking the limit $N\to\infty$ yields an integral of the form

$$S=\left|\frac{\gamma E_0^3}{L}\int_0^L dx \exp\left(-\frac{3}{2}\alpha x-\frac{1}{2}\alpha(L-x)\right)\right|^2, \tag{A5}$$

and rearranging gives,

$$S=\left|\frac{\gamma E_0^3}{L}\exp\left(-\frac{\alpha L}{2}\right)\int_0^L dx \exp(-\alpha x)\right|^2. \tag{A6}$$

Evaluation of the integral yields,

$$S=\left|\frac{\gamma E_0^3}{\alpha L}\exp\left(-\frac{\alpha L}{2}\right)[1-\exp(-\alpha L)]\right|^2. \tag{A7}$$

The only complex quantity in Eq. (A7) is the electric field. Taking the absolute value squared gives the intensity. Then,

$$S=\gamma^2 I_0^3 \exp(-A)\left\{\frac{[1-\exp(-A)]}{A}\right\}^2, \tag{A8}$$

where $\alpha l=A$, the absorbance.

Normalization for the inner filter effect of the VES must be performed at each wavelength since the absorbance is wavelength dependent, $A(\omega)$. $A(\omega)$ is determined by a conventional IR spectrum. If the laser intensity varies with wavelength, then $I_0^3(\omega)$ can be measured as the laser wavelength is scanned. The inner filter wavelength normalization factor, $N(\omega)$, is a relative scaling of the spectrum and is independent of the factors contained in γ that determine the absolute size of the spectrum. Therefore, the inner filter wavelength dependent normalization factor is

$$N(\omega)=I_0^3(\omega)\exp(-A(\omega))\left\{\frac{[1-\exp(-A(\omega))]}{A(\omega)}\right\}^2. \tag{A9}$$

[1] K. D. Rector, A. S. Kwok, C. Ferrante, R. S. Francis, and M. D. Fayer, Chem. Phys. Lett. **276**, 217 (1997).
[2] K. D. Rector, C. W. Rella, A. S. Kwok, J. R. Hill, S. G. Sligar, E. Y. P. Chien, D. D. Dlott, and M. D. Fayer, J. Phys. Chem. B **101**, 1468 (1997).
[3] C. W. Rella, K. D. Rector, A. S. Kwok, J. R. Hill, H. A. Schwettman, D. D. Dlott, and M. D. Fayer, J. Phys. Chem. (London) **100**, 15620 (1996).
[4] A. Tokmakoff and M. D. Fayer, J. Chem. Phys. **103**, 2810 (1995).
[5] A. Tokmakoff, D. Zimdars, R. S. Urdahl, R. S. Francis, A. S. Kwok, and M. D. Fayer, J. Phys. Chem.(London) **99**, 13310 (1995).
[6] S. Mani, J. Pauly, S. Conolly, C. Meyer, and D. Nishimura, Magn. Reson. Med. **37**, 898 (1997).
[7] X. Yang and L. W. Jelinski, J. Magn. Reson., Ser. B **107**, 1 (1995).
[8] E. L. Hahn, Phys. Rev. **80**, 580 (1950).
[9] K. Rahmelow and W. Hübner, Appl. Spectrosc. **51**, 160 (1997).
[10] A. Elliot and E. J. Ambrose, Nature (London) **165**, 921 (1950).
[11] W. K. Surewicz and H. H. Mantsch, ''Infrared absorption methods for examining protein structure,'' in *Spectroscopic Methods for Determining Protein Structure in Solution*, edited by H. A. Havel, (VCH Publishers, New York, 1996), pp. 135.
[12] P. E. Saarinen, Appl. Spectrosc. **51**, 188 (1997).
[13] K. D. Rector and M. D. Fayer, Int. Rev. Phys. Chem. (in press).
[14] P. C. Chen, J. P. Hamilton, A. Zilian, M. J. Labuda, and J. C. Wright, Appl. Spectrosc. **52**, 380 (1998).
[15] R. G. Gordon, J. Chem. Phys. **43**, 1307 (1965).
[16] R. G. Gordon, Adv. Magn. Reson. **3**, 1 (1968).
[17] B. J. Berne, *Physical Chemistry: An Advanced Treatise* (Academic, New York, 1971), Vol. VIIIB.
[18] D. W. Oxtoby, Annu. Rev. Phys. Chem. **32**, 77 (1981).
[19] E. B. Wilson, Jr., J. C. Decius, and P. C. Cross, *Molecular Vibrations: The Theory of Infrared and Raman Vibrational Spectra* (McGraw-Hill, New York, 1955).
[20] N. A. Kurnit, I. D. Abella, and S. R. Hartmann, Phys. Rev. Lett. **13**, 567 (1964).
[21] I. D. Abella, N. A. Kurnit, and S. R. Hartmann, Phys. Rev. Lett. **14**, 391 (1966).
[22] T. C. Farrar and D. E. Becker, *Pulse and Fourier Transform NMR* (Academic, New York, 1971).
[23] D. T. Leeson and D. A. Wiersma, Phys. Rev. Lett. **74**, 2138 (1995).
[24] D. T. Leeson, D. A. Wiersma, K. Fritsch, and J. Friedrich, J. Phys. Chem. B **101**, 6331 (1997).
[25] Y. S. Bai and M. D. Fayer, Phys. Rev. B **39**, 11066 (1989).
[26] H. C. Meijers and D. A. Wiersma, J. Lumin. **53**, 80 (1992).
[27] H. W. H. Lee, A. L. Huston, M. Gehrtz, and W. E. Moerner, Chem. Phys. Lett. **114**, 491 (1985).
[28] J. M. Hayes, R. P. Stout, and G. J. Small, J. Chem. Phys. **74**, 4266 (1981).
[29] R. M. Macfarlane and R. M. Shelby, Opt. Commun. **45**, 46 (1983).
[30] M. Berg, C. A. Walsh, L. R. Narasimhan, K. A. Littau, and M. D. Fayer, J. Chem. Phys. **88**, 1564 (1988).
[31] R. F. Loring and S. Mukamel, J. Chem. Phys. **83**, 2116 (1985).
[32] M. Berg, C. A. Walsh, L. R. Narasimhan, K. A. Littau, and M. D. Fayer, J. Chem. Phys. **88**, 1564 (1988).
[33] K. D. Rector, A. S. Kwok, C. Ferrante, A. Tokmakoff, C. W. Rella, and M. D. Fayer, J. Chem. Phys. **106**, 10027 (1997).
[34] A. Tokmakoff, A. S. Kwok, R. S. Urdahl, R. S. Francis, and M. D. Fayer, Chem. Phys. Lett. **234**, 289 (1995).
[35] E. Geva and J. L. Skinner, J. Chem. Phys. **107**, 7630 (1997).
[36] S. Mukamel and R. F. Loring, J. Opt. Soc. Am. B **3**, 595 (1986).
[37] Y. J. Yan and S. Mukamel, J. Chem. Phys. **94**, 179 (1991).
[38] D. A. Zimdars, ''Optical Dephasing and Spectral Diffusion in Organic Liquids and Glasses as Studied by Photon Echo Spectroscopies: Experiment and Theory,'' Graduate Thesis, Stanford University (1996).
[39] S. Mukamel, *Principles of Nonlinear Optical Spectroscopy* (Oxford University Press, New York, 1995).
[40] D. A. Zimdars, R. S. Francis, C. Ferrante, and M. D. Fayer, J. Chem. Phys. **106**, 7498 (1997).
[41] K. D. Rector and M. D. Fayer (unpublished).
[42] K. D. Rector, J. R. Engholm, J. R. Hill, D. J. Myers, R. Hu, S. G. Boxer, D. D. Dlott, and M. D. Fayer, J. Phys. Chem. B **102**, 331 (1998).
[43] K. D. Rector, D. D. Dlott, and M. D. Fayer (unpublished).
[44] R. H. Austin, K. Beeson, L. Eisenstein, H. Frauenfelder, I. C. Gunsalus, and V. P. Marshal, Phys. Rev. Lett. **32**, 403 (1974).
[45] A. Ansari, J. Beredzen, D. Braunstein, B. R. Cowen, H. Frauenfelder, M. K. Hong, I. E. T. Iben, J. B. Johnson, P. Ormos, T. Sauke, R. Schroll, A. Schulte, P. J. Steinback, J. Vittitow, and R. D. Young, Biophys. Chem. **26**, 337 (1987).
[46] J. R. Hill, D. D. Dlott, C. W. Rella, T. I. Smith, H. A. Schwettman, K. A. Peterson, A. S. Kwok, K. D. Rector, and M. D. Fayer, Biospectroscopy **2**, 227 (1996).